Neuron, Volume *74*

Supplemental Information

Mg^{2+} Block of *Drosophila* NMDA Receptors Is Required for Long-Term Memory Formation and CREB-Dependent Gene Expression

Tomoyuki Miyashita, Yoshiaki Oda, Junjiro Horiuchi, Jerry C.P. Yin, Takako Morimoto, and Minoru Saitoe

Inventory of Supplemental Information

Table S1. Primer Sequences for Real-Time PCR

	Upstream	Downstream
activin	5’-TGGCAAAAATGGTGAGATGA-3’	5’-TCCAATGCTAGAGCGACCTT-3’
homer	5’-CGAACAACCGATTTTCACCT-3’	5’-CTAACGTTGACCGCCTTCAT-3’
staufen	5’-CACCAACCAACGAAACACAG-3’	5’-GTTGCTACCATGGGCACTTT-3’
RP-49	5’-CACCGGATTCAAGAAGTTCC-3’	5’-GACAATCTCCTTGCGCTTCT-3’
dlg	5’-CCACCACAACTTGGACACTG-3’	5’-ATTTGTTGCTGCTGCTGTTG-3’
14-3-3ζ	5’-AAAACCAAAATGCAGCCAAC-3’	5’-CCAATTGGCAAGCTTTGTCT-3’
dCREB2	5’-CCAATGACGTGGTCGATGT-3’	5’-CTTTGTGGGTTCTGTTGCTG-3’
dCREB2-b	5’-TGCAGTGCAAATCCCTCCAA-3’	5’-CCGCTGTTGTCGCTCATGTC-3’

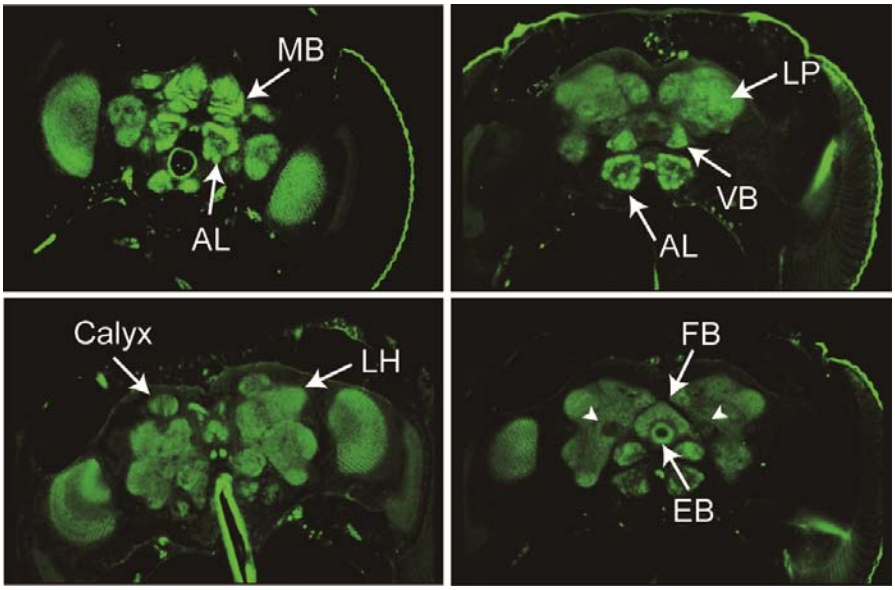

Figure S1. Distribution of the dNR1 subunit in the *Drosophila* brain.

Immunofluorescence images using antibody directed against a C-terminal peptide sequence of dNR1 (αNM1) show that dNR1 is expressed throughout the fly brain, including the calyces (Calyx) and lobes of the mushroom bodies (MB), antennal lobes (AL), lateral protocerebrum (LP), ventral body (VB), lateral horn (LH), and the fanshaped body (FB) and ellipsoid body (EB) of the central complex. Note that the mushroom body peduncles (arrow heads), axonal regions of the mushroom body complex show reduced dNR1 signal.

(This figure is relevant to Figure 1 in the main text)

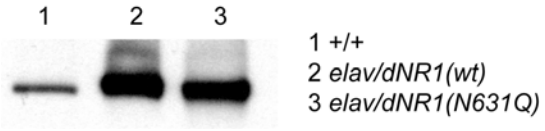

Figure S2. Overexpression of dNR1(wt) and dNR1(N631Q).

A western blot probed with αNM1 antibody shows prominent increases in dNR1 in *elav-GAL4/UAS-dNR1(wt)-W5* [*elav/dNR1(wt)*] and *elav-GAL4/UAS-dNR1(N631Q)-M15* [*elav/dNR1(N631Q)*] flies compared to wild-type [+/+].

(This figure is relevant to Figure 2 in the main text)

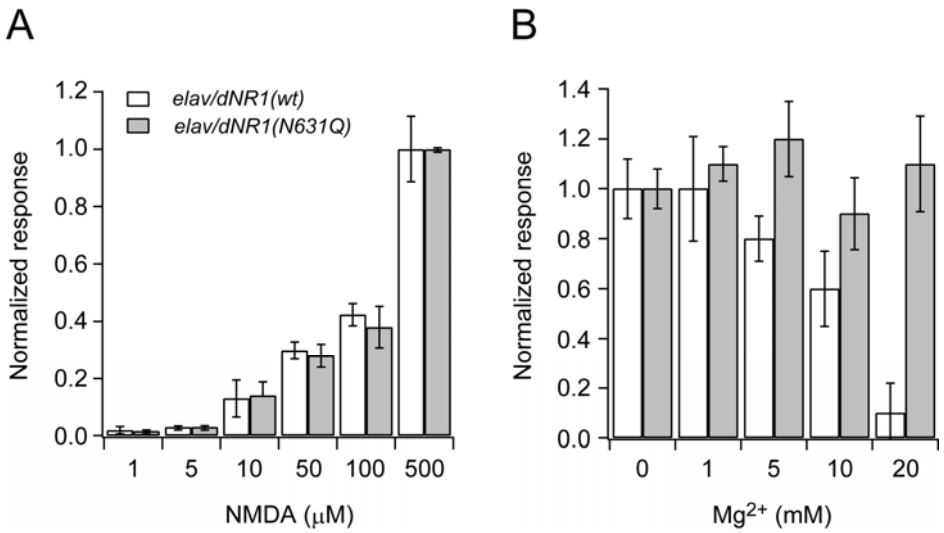

Figure S3. NMDA and Mg^{2+} dose response curves.

(A) Normalized responses of neurons expressing dNR1(wt) and dNR1(N631Q) subunits to increasing concentrations of NMDA. Currents were recorded at a membrane potential of -80 mV in the absence of Mg^{2+}. No differences were observed between dNR1(wt) and dNR1(N631Q) expressing cells. N = 4-6 for all data.

(B) Suppression of NMDAR responses at different Mg^{2+} concentrations. NMDAR currents were induced using 100 μM NMDA at a membrane potential of -80 mV. Responses are inhibited by increasing [Mg^{2+}] in *elav/dNR1(wt)* cells while responses are unaffected by [Mg^{2+}] in *elav/dNR1(N631Q)* cells. N = 4-6 for all data.

(This figure is relevant to Figures 2 and 3 in the main text)

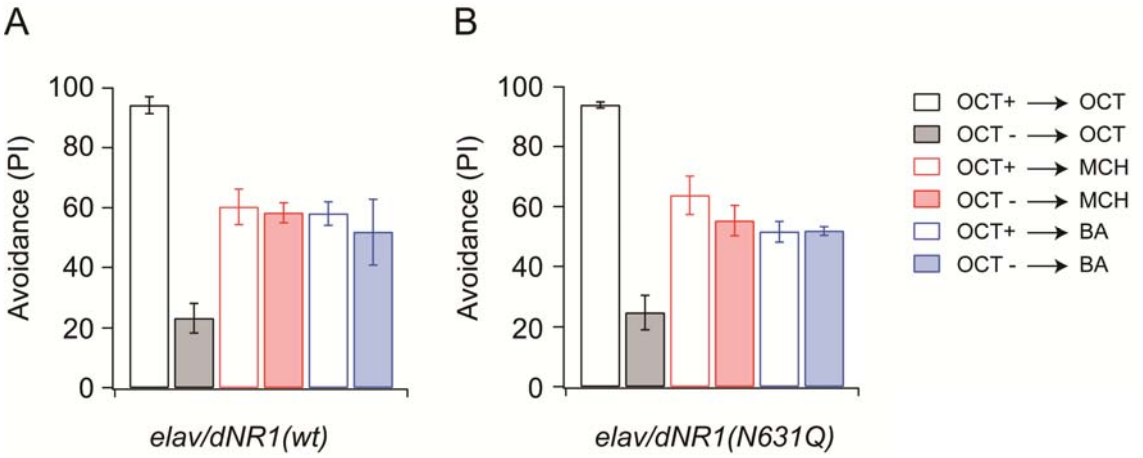

Figure S4. Mg^{2+} block mutations do not alter odor specificity of learned olfactory associations.

(A, B) Flies were exposed to 4-octanol with (OCT+), or without (OCT-) simultaneous electric shocks. Immediately after training, flies were placed in a T-maze, where they were given a choice between an odor (OCT, 4-methylcyclohexanol (MCH) or benzaldehyde (BA)) and air. Trained *elav/dNR1(wt)* flies exposed to the OCT+ condition avoid OCT much more those exposed to the OCT- condition. There is no difference between *elav/dNR1(wt)* flies exposed to the OCT+ or OCT- condition for responses to MCH or BA, indicating that training to one odor does not affect responses to an unrelated odor. In all conditions, responses of *elav/dNR1(N631Q)* flies were not different from those of *elav/dNR1(wt)* flies suggesting that odor specificity is not altered by mutations which abolish Mg^{2+} block. N = 8-10 for all samples.

(This figure is associated with Figure 4 in the main text)

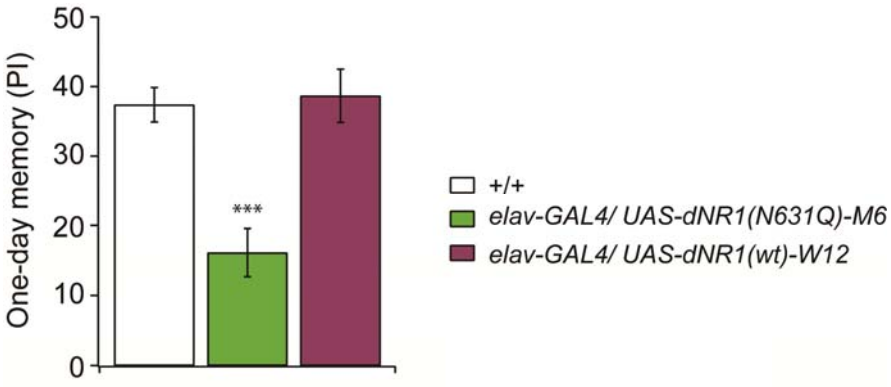

Figure S5. LTM defects in *elav-GAL4/UAS-dNR1(N631Q)-M6* flies.

Similar to *elav-GAL4/UAS-dNR1(N631Q)-M15* [*elav/dNR1(N631Q)*] flies (see Fig. 3), one-day memory after spaced training is significantly reduced (*** $P < 0.0001$) in *elav-GAL4/UAS-dNR1(N631Q)-M6* flies while it is normal in *elav-GAL4/UAS-dNR1(wt)-W12* flies. These results indicate that expression of a *dNR1(N631Q)* transgene in neurons disrupts LTM formation independent of insertion site. N = 10 for all data.

(This figure supports Figure 3C in the main text)

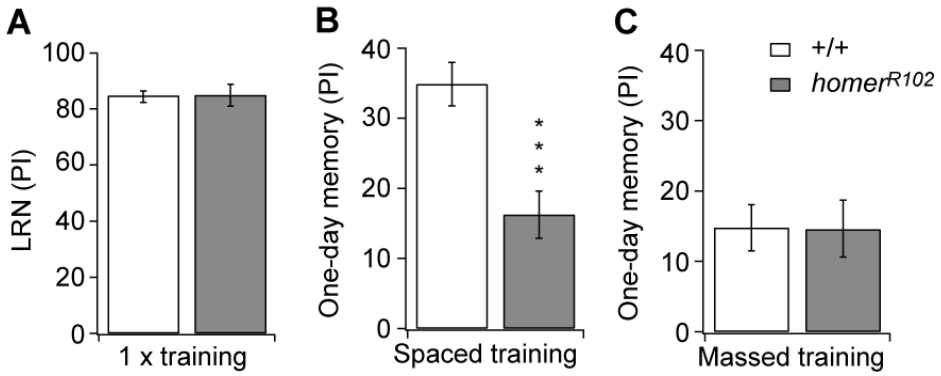

Figure S6. LTM defects in *homer* mutants.

(**A**) Learning (LRN) after single cycle training is indistinguishable in *homer* and wild-type (+/+) flies. N = 6 for all data.

(**B, C**) One-day memory after spaced training is significantly reduced in *homer* mutants (B), while one-day memory after massed training is normal (**C**), indicating that homer is required for LTM but not ARM. ***, P < 0.001 by t-test, N = 10 for all data.

(This figure supports Figure 6 in the main text)

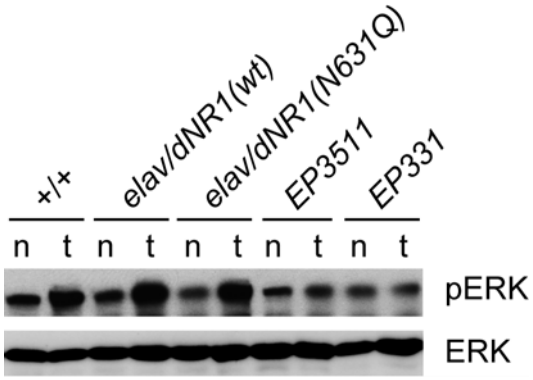

Figure S7. Training-dependent increases in MAPK phosphorylation are not disrupted in *elav/dNR1(N631Q)* flies.

In contrast to hypomorphic dNR1 mutants (*EP3511* and *EP331*), ERK activity, monitored as phosphorylated ERK, increases normally after spaced training in *elav/dNR1(N631Q)* flies, suggesting that Ca^{2+} signaling during correlated activity is not disrupted in the absence of Mg^{2+} block. n = extracts from naive flies; t = extracts from spaced trained flies.

Immunoblotting was performed as described previously (Pagani et al., 2009). Five fly heads of each genotype were harvested immediately after training and used for immunoblotting.

(This figure is relevant to Figure 8 in the main text)

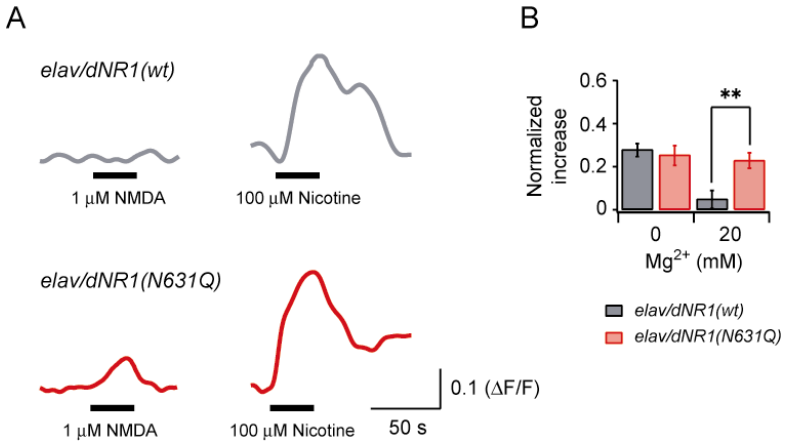

Figure S8. Increased Ca^{2+} influx in Mg^{2+} block mutants upon NMDA stimulation.

(**A**) Changes in fluorescent intensity of fluo-3 ($\Delta F/F_0$) in neurons upon addition of NMDA or nicotine. 1 μM NMDA or 100 μM nicotine was applied in the presence of 20 mM extracellular Mg^{2+} to neurons from pupae of the indicated genotypes. Neurons were loaded with fluo-3-AM prior to NMDA or nicotine addition.

(**B**) Mg^{2+} block-mediated changes in $[Ca^{2+}]_i$. The peak change ($\Delta F/F_0$) upon application of 1 μM NMDA was normalized to the peak change ($\Delta F/F_0$) upon application of 100 μM nicotine. As seen in (**A**), 1 μM NMDA elicited a significant increase in $[Ca^{2+}]_i$ in neurons from *elav/dNR1(N631Q)* pupae but not in neurons from *elav/dNR1(wt)* pupae in the presence of 20 mM Mg^{2+}. N = 8 for all data.

(This figure is related to Figure 7 in the main text)

Supplemental Experimental Procedures for Ca^{2+} Imaging (Figure S8)

A confocal laser microscope system (Fluoview FV500, Olympus) was used for imaging. Primary cultured neurons from pupal brains were loaded with an acetoxymethyl (AM) ester form of fluo-3 (excitation wavelength at 488 nm) at 10 μg/ml as described in (Saitoe et al., 1998) and washed with standard extracellular HL-3 solution. To minimize photodynamic damage to cells and photobleaching, laser intensity was set to 0.1%.

Changes in fluorescence intensity of fluo-3 in soma were expressed as $\Delta F/F_0 = (F - F_0)/F_0$, where F_0 is the baseline fluorescence intensity measured for 50 ms prior to the stimulus, and F is the peak fluorescence intensity upon addition of drug. Since nicotinic acetylcholine receptors are widely distributed in the adult brain, $\Delta F/F_0$ induced by NMDA stimulation was normalized to that induced by nicotine stimulation.

Supplemental References

Pagani, M.R., Oishi, K., Gelb, B.D., and Zhong, Y. (2009). The phosphatase SHP2 regulates the spacing effect for long-term memory induction. Cell *139*, 186-198.

Saitoe, M., Koshimoto, H., Hirano, M., Suga, T., and Kidokoro, Y. (1998). Distribution of functional glutamate receptors in cultured embryonic Drosophila myotubes revealed using focal release of L-glutamate from caged compound by laser. J Neurosci Methods *80*, 163-170.